Published in final edited form as:
Neuroimage. 2012 August 15; 62(2): 1299–1310. doi:10.1016/j.neuroimage.2012.01.032.

The Future of the Human Connectome

D.C. Van Essen[1] and **K. Ugurbil**[2]
[2]University of Minnesota Center for Magnetic Resonance Research 2021 6th Street, SE Minneapolis, MN 55455

Abstract

The opportunity to explore the human connectome using cutting-edge neuroimaging methods has elicited widespread interest. How far will the field be able to progress in deciphering long-distance connectivity patterns and in relating differences in connectivity to phenotypic characteristics in health and disease? We discuss the daunting nature of this challenge in relation to specific complexities of brain circuitry and known limitations of in vivo imaging methods. We also discuss the excellent prospects for continuing improvements in data acquisition and analysis. Accordingly, we are optimistic that major insights will emerge from human connectomics in the coming decade.

Keywords

Brain; Magnetic Resonance Imaging; MRI; connectivity; tractography; functional imaging; fMRI; resting state; diffusion imaging; multiband; ultrahigh field imaging; 7 Tesla

1. Introduction

The Human Connectome Project (HCP) is an ambitious effort to chart human brain connectivity in a large population of healthy adults using cutting-edge neuroimaging methods. In the context of the HCP of this project, a connectome (or, more properly, a ‘macro-connectome’) is a comprehensive description of the connections between every gray matter location and every other gray matter location at the macroscopic scale (~1 mm^3 or greater) as analyzed using noninvasive neuroimaging. It is distinct from the ‘micro-connectome’ realm, which aims to comprehensively chart connectivity at the level of individual neurons and synapses but is currently restricted to sub-millimeter brain regions in laboratory animals (Briggmann et al., 2011; Bock et al., 2011; Lichtman and Sanes, 2008). Through the HCP and other macro-connectome efforts, rapid progress can be expected on many methodological fronts, coupled with the acquisition of enormous amounts of data. This will open up a new era in exploring the human connectome and its relationship to behavior.

1.1. Vignettes from the ‘pre-connectome’ era

As a prelude to discussing the future of the human connectome, it is appropriate for this special issue to reflect briefly on the state of primate connectivity studies two decades ago,

[1]Corresponding Author Washington University School of Medicine Anatomy & Neurobiology 660 S. Euclid Avenue St. Louis, MO 63128 314-362-7043 tel 314-747-3436 - fax vanessen@wustl.edu.

when fMRI was born. One of the authors (DVE) had just published a map of cortical areas and an analysis of cortical connectivity in macaque visual cortex (Fig. 1) in which evidence was reported for several hundred cortico-cortical connections linking 32 visual areas (Felleman & Van Essen, 1991). This circuitry was much more complex than many neuroscientists had anticipated, yet important organizational principles could be elucidated by considering the pattern of connections within the overall 32 × 32 connectivity matrix (a 'parcellated connectome' in current parlance). Around this time, the other author (KU) was laying the foundations of fMRI as a tool for studying human brain function (Ogawa et al., 1992; Tank et al., 1992; Ugurbil, this issue). The first fMRI studies were considered a success when any cortical activation was detected using full-field or hemifield visual stimulation. Nevertheless, it was apparent from the outset that fMRI offered great potential for elucidating human brain function; developing it to the point of mapping the cortical areas identified by DVE (Fig. 1) was an objective frequently mentioned by KU. There were even clues early on that spontaneous fluctuations in the fMRI BOLD signal might enable exploration of functional connectivity. Specifically, Ogawa et al. (1993) commented "If [these] oscillations represent a neural origin, it may be possible to measure spatial correlations of the responses across the cortex. This would provide an MRI method of mapping patterns of functional connections between cortical areas." However, the notion that a comprehensive high-resolution mapping of brain connectivity would be feasible using fMRI in particular or, for that matter, any other MR-based method would have been considered far-fetched at the time. Indeed, around that time Francis Crick and Ted Jones bemoaned the lack of promising methods for exploring long-distance connections in the human brain (Crick and Jones, 1993).

Remarkable advances on many fronts now make it feasible to decipher fundamental aspects of the human connectome and its variability in health and disease. Two methods in particular can be used to make strong, albeit indirect, inferences about brain connectivity. The first, diffusion imaging (dMRI), estimates the orientation of fiber bundles in white matter based on anisotropies in water diffusion. It provides the inputs for tractography analyses that can be used to infer '*structural connectivity*' between gray matter regions (Wansapura et al., 1999; Jbabdi and Johansen-Berg, 2011). Sporns et al. (2005) first proposed that tractography could be used for a systematic investigation of the human connectome and its variability. The second method, resting-state fMRI (R-fMRI), uses temporal correlations in the slow fluctuations of the BOLD fMRI signal to infer '*functional connectivity*'. R-fMRI serves as an indirect but nonetheless invaluable indicator of gray-matter regions that interact strongly and in many cases are connected anatomically (Biswal et al., 1995; Fox and Raichle, 2007; Vincent et al., 2007; Beckmann et al., 2005; Smith, 2011). A growing number of studies have revealed important insights through systematic analyses of whole-brain connectivity using dMRI and/or R-fMRI. This includes analyses of brain networks, modularity, and hubs, as well as demonstration of connectivity-based parcellation (Hagmann et al. 2008; Van den Heuvel and Hulshoff, 2010; Cohen et al., 2008; Nelson et al., 2010; Yeo et al., 2011; Mars et al., 2011; Power et al., 2011).

Despite their promise and potential, current methods for assessing structural and functional connectivity face serious technical limitations at multiple levels. Analyses of structural connectivity must cope with a high incidence of false positives and false negatives, combined with an inherent difficulty in making quantitative estimates of connection strength (Iturria-Medina et al., 2008; Jones and Cercignani, 2010; Jbabdi and Johansen-Berg, 2011). Analyses of functional connectivity are limited by the indirect nature of neurovascular coupling to neural activity and the presence of confounding long-range correlations of vascular origin (Mitra et al., 1995). In addition, functional correlations reflect more than direct anatomical connectivity (Vincent et al., 2007), as they can be influenced by common inputs and/or interactions via serially connected areas. Both approaches also face limitations

imposed by the difficulty of accurately parcellating the brain into functionally distinct subdivisions (parcels) and in aligning data across subjects (intersubject registration).

1.2. Early days of the HCP

Given the uniqueness of the Human Connectome Project, a few comments on its origins and early days are warranted. In the summer of 2009, a Request For Applications (RFA) was announced by the NIH Neuroscience Blueprint Institutes and Centers, with the intent of awarding a single large grant to characterize the human connectome in 'up to hundreds' of healthy adults. The rationale for launching such a bold plan at that time was based on the impressive technological advances in neuroimaging just described, coupled with the prospect of accelerating progress by a judicious investment of resources. Importantly in this regard, the RFA encouraged the use of multiple imaging methodologies and allowed for an extended period for optimizing and refining the data acquisition and analysis methods, rather than relying on state-of-the-art at the time of the grant award. It also mandated that the resultant datasets be made freely available via a robust and user-friendly informatics platform. Many neuroscientists and NIH leaders contributed to the framing of the HCP RFA, but Mike Huerta (then at NIMH) deserves special recognition for his central role in articulating and advocating the vision.

NIH ultimately awarded two complementary HCP grants (http://humanconnectome.org/consortia/). The authors are PI's for the 'WU-Minn' HCP consortium, led by Washington University and University of Minnesota and involving several dozen investigators from 11 institutions. This is a 5-year, $30M effort to chart the human connectome and its variability in 1,200 healthy adults (twins and their non-twin siblings) using dMRI, R-fMRI, Task-fMRI, and MEG/EEG. A smaller 3-year grant was awarded to a consortium involving Massachusetts General Hospital (MGH) and UCLA, with a focus on developing a 'next-generation' 3T MR scanner for diffusion imaging.

From a personal perspective, we have found it extremely rewarding to bring together an extraordinarily talented multidisciplinary team of enthusiastic and dedicated investigators. This team was able in a few months to formulate a high-level vision, translate it into a detailed concept for the many sub-projects needed for eventual success of the HCP, and even generate promising preliminary data using the complementary expertise among consortium members. Since the grant was awarded, the excitement of moving forward has been coupled with a sobering appreciation of the daunting scope of the endeavor. Currently, 84 consortium members work on the WU-Minn project (36 investigators, plus students, postdocs, and technical staff). Each consortium member participates in at least one of seven operational teams (from pulse-sequence development to informatics - http://www.humanconnectome.org/about/teams.html) plus various ad hoc working groups established to deal with concrete issues. Coordination of these efforts is facilitated by a full-time project manager, intensive 2-day 'All-Hands' meetings (two held to date), regular meetings of a Steering Committee and an Operations Committee, monthly 'science' teleconference meetings to keep the consortium apprised of ongoing progress, and countless emails, conference calls, and ad hoc small-group meetings to address specific issues. This has enabled rapid progress on many fronts during the early stages of the project (e.g., Feinberg et al., 2010; Marcus et al., 2011; Van Essen et al., 2011c; Power et al., 2011). Critical to this progress has been an excellent esprit de corps and high level of commitment among all members of the consortium.

In the remainder of this article we concentrate on two complementary topics. The first addresses a number of neurobiological issues that are relevant to elucidating human brain connectivity. They provide a sobering reminder of many facets of the overall problem, but also suggest profitable directions to pursue in meeting these challenges. The second topic

highlights some of the advances to be anticipated via methodological improvements in MR data acquisition and analysis. Other aspects of the HCP endeavor that are important for its success are outside the scope of this article; many of these are covered elsewhere (Marcus et al., 2011; Van Essen et al., 2011c; Behrens and Sporns, 2011; Akil et al., 2011). Our overarching objective is to provide a better appreciation of the types of advances in human connectomics that can be anticipated in the coming decade as well as the limitations that will be difficult to overcome in this time frame.

2. Neurobiological considerations and constraints

Human brain circuitry is extraordinarily complex by any measure. Here, we discuss specific aspects of the brain's complexity that are critical for deciphering the human connectome and yet may not be widely recognized. (i) *Scales of analysis.* In vivo neuroimaging enables exploration of connectivity at a scale that is fine-grained relative to overall brain dimensions, but it is extremely coarse in relation to the brain's cellular components. (ii) Brain *parcellations.* The human brain contains hundreds of distinct parcels that differ in their architecture, connectivity, and/or function, yet our understanding of their layout is woefully incomplete. (iii) *Long-distance anatomical connectivity.* Principles of long-distance connectivity determined in nonhuman primates have major and somewhat unexpected implications for understanding the human connectome. (iv) *Axonal trajectories.* Information about the trajectories of fiber bundles and individual axons within white matter is critical for the analysis and interpretation of structural connectivity using diffusion imaging, yet surprisingly little is known about these trajectories from animal studies. (v) Functional connectivity and *neurovascular coupling.* The complex nature of neurovascular coupling, including the spatial relationship between BOLD fMRI signals and underlying patterns of neuronal activity, has a major impact on the interpretation of functional connectivity studies. (vi) *Individual variability.* The high degree of individual variability, especially of the convoluted cerebral cortex, poses major challenges for connectome analyses, yet it also offers a great opportunity for exploring the neural basis of individual differences over a wide range of behavioral phenotypes.

2.1. Scales of analysis

In considering spatial scales (and reflecting our penchant for neuroanatomical quantification!), it is useful to summarize key facts about major components of the human brain (Table 1). For the cerebral cortex, each of the two topologically separate hemispheres is a highly convoluted sheet with average thickness of ~2.4 mm and surface area of ~1,000 cm^2 (Van Essen et al., 2011b), about the size of a medium pizza. Cerebellar cortex is a single, topologically continuous sheet spanning both hemispheres. It is only ~1 mm thick and has an estimated surface area of ~1,100 cm^2, comparable to that of an individual cerebral hemisphere. Subcortical structures (including basal ganglia, thalamus, brainstem) occupy ~80 cm^3, one-sixth the volume of cerebral cortical gray matter. Subcortical white matter, i.e., the long-distance cables between gray-matter regions, occupies ~400 cm^3, more than half the volume of the combined gray matter structures.

To characterize brain circuitry as accurately as possible, it is desirable to analyze structural and functional connectivity across the whole brain at the finest spatial resolution supported by the data acquisition and analysis methods. This leads to the concept of a '*dense connectome*' as a fine-grained connectivity matrix between each gray matter voxel or surface vertex and every other gray matter voxel or vertex (Marcus et al., 2011). At the spatial resolution supported by conventional 3T R-fMRI data acquisition (3 mm cubic voxels), a dense connectome can be represented by a matrix of ~45,000 × 45,000 elements. Analysis and visualization of dense connectome datasets are facilitated by the new 'CIFTI' data format (http://www.nitrc.org/projects/cifti/) that can handle surface vertices and gray

matter voxels in a single data file (Marcus et al., 2011). Methodological improvements discussed below should substantially improve resolution, resulting in much larger dense connectome datasets, for example, just improving the resolution to 2 mm voxel dimensions results in a dense connectome exceeding over 90,000 × 90,000 elements.

At a cellular level, cerebral neocortex contains on average ~90,000 neurons per mm^2 surface area and white matter contains ~300,000 axons/mm^3 (Table 1). The density of synapses is far greater (~$3 \times 10^8/mm^3$). Hence, even with the most optimistic scenarios for improved spatial resolution, a vast gulf will remain between the macro-connectome domain of in vivo neuroimaging and the micro-connectome domain dealing with the 3D arrangement of neurons, axons, dendrites, synapses, and glia.

2.2. Brain parcellations

The analysis of dense connectomes will be one major thrust of human connectome studies. However, many analyses will capitalize on more compact representations provided by 'parcellated connectomes' that describe average connectivity between different brain subregions (parcels). It is obviously important to have parcellation schemes that are as accurate as possible, so that connectivity patterns can be related to functionally meaningful parcels (Wig et al., 2011; Behrens and Sporns, 2011). The challenges in meeting this objective differ for each brain region.

Cerebral cortex contains a mosaic of many different areas that are distinct in their architecture, topography, connectivity, and/or function (Felleman & Van Essen, 1991). Despite a century of progress, determining the precise layout of cortical areas is far from complete, even for the intensively studied macaque monkey. By one recent estimate, there are ~140 distinct neocortical and transitional areas in each hemisphere of the macaque (Van Essen et al., 2011a). Human cortex may contain 150 - 200 areas/hemisphere, based on accurate maps of 52 areas that encompass ~1/3 of neocortical surface area (Fig. 2; Van Essen et al., 2011b). The spatial extent of accurately mapped human areas averages ~7 cm^2 per parcel; but in both humans and macaques cortical areas span a more than 100-fold range in average surface area.

Subcortical gray matter includes a handful of major structures (basal ganglia, thalamus, hypothalamus, midbrain, and brainstem) that can be segmented using structural MR. Each of these structures contain numerous finer-grained parcels (nuclei and subnuclei) that are more difficult to delineate. The total number that are large enough to be identifiable using in vivo neuroimaging is approximately 75 on each side of the brain (cf. Mai et al., 2007).

Cerebellar cortex has proven difficult to parcellate because it is remarkably uniform in its cellular architecture, completely lacks cortico-cortical connections, and is connected to other brain regions via compact, poorly understood nuclei (Strick et al., 2009). Nonetheless, it is functionally heterogeneous and contains multiple topographically organized subdivisions. Buckner et al., (2011) used a functional connectivity analysis to infer that cerebellar cortex contains three 'homotopic' maps of the 'full cerebrum' (most of the neocortical sheet). Within this coarse mapping, they identified cerebellar subregions corresponding to each of 17 networks and many more spatially discrete subregions previously derived from a functional connectivity analysis of cerebral cortex (Yeo et al., 2011). Altogether, it seems likely that there are at least 20 and perhaps 50 or more functionally distinct cerebellar parcels (Table 1).

In aggregate, these observations suggest that the human brain contains about 500 (+/- 100) neurobiologically distinct parcels accessible to in vivo neuroimaging. A connectivity matrix based on such a parcellation would have roughly 25,000 (+/- ~10,000) possible entries.

Information from nonhuman primates provides important constraints on the connectivity patterns to be expected within this matrix.

2.3. Long-distance anatomical connectivity

Even though white-matter tracts have been studied in humans for more than a century, there is very little hard evidence ('ground truth') on the detailed pattern of long-distance connections between gray-matter regions. However, a wealth of relevant data comes from anatomical tracer studies in nonhuman primates. For cerebral cortex, quantitative analyses of cortico-cortical connections from retrograde tracer injections in the macaque are especially informative. Four general observations warrant mention. (i) *Numerous cortical inputs and outputs*. Areas V1, V2, and V4 each receive inputs from 25 other cortical areas within the same hemisphere (Markov et al., 2011), which is many more than were reported in previous studies. The number of inputs to any given area in temporal, parietal, and frontal cortex is even greater (H. Kennedy, N. Markov, personal communication; Lewis and Van Essen, 2000; Gerbella et al., 2010, 2011). There are also numerous interhemispheric connections though these are not as well studied (e.g., Lewis & Van Essen, 2000). (ii) *Wide range of connection strengths*. Remarkably, the inputs to each area span more than five orders of magnitude in strength, as assessed by the fraction of labeled neurons, yet the connection strength from any given area is reproducible, within 1 – 2 orders of magnitude, when tested by repeat injections (Markov et al., 2011). (iii) *Similar connectivity profiles for adjacent areas.* The connectivity profiles for foveal portions of areas V1, V2, and V4 are strikingly similar in terms of the other areas to which they are connected; the differences are mainly quantitative (strength of inputs) rather than qualitative (Markov et al., 2011). (iv) *Within-area heterogeneity.* The connectivity of an individual cortical area can show considerable internal heterogeneity. For example, large regional differences in the connectivity of topographically organized areas have been demonstrated for central vs. peripheral vision in extrastriate cortex (Baizer et al., 1991) and for somatotopic sensory and motor areas (He et al., 1993, 1995). In addition, some visual areas, including V1, V2, and V4, have a finer-grained, repetitive modular substructure with distinct connectivity patterns (Livingstone and Hubel, 1984; DeYoe et al., 1994; Sincich et al., 2010). Such heterogeneity has major implications for using connectivity to distinguish among cortical areas.

Analogous issues arise in considering the many complex pathways that involve subcortical structures and the cerebellum. In the interests of brevity, these are not considered further here, except to emphasize the need to interpret human connectivity studies in relation to the full set of anatomical realities inferred from nonhuman primate connectivity studies.

Extrapolating from these observations on the parcellated macaque connectome to human cortex suggests that a large fraction (possibly half or more) of the possible cortico-cortical connections within each hemisphere might actually exist. However, most of these pathways are likely to be weak and may be difficult to detect reliably. The complexity will be even greater when considering connections between the two hemispheres and among subcortical structures. In short, the parcellated human connectome is likely to be a highly distributed network in which each parcel has many inputs and outputs (perhaps 100 or more of each), most of which are relatively weak. Hence, it is of paramount importance to have *in vivo* imaging methods that can chart complex connectivity patterns quantitatively and with high spatial fidelity. This will require improvements in sensitivity, spatial resolution, acquisition time, and analysis methods (see Section 3).

2.4 Axonal trajectories

Tractography analyses based on diffusion imaging estimate the trajectories of fiber bundles that have coherent orientations (i.e., are approximately collinear) across adjacent white

matter voxels. When using tractography to infer connectivity between distant gray matter regions, a critical assumption is that the axons mediating the anatomical pathway are tightly fasciculated along their entire length - even in regions where crossing fibers occur. This assumption is supported to a limited degree by classical dissections of human white matter (Déjérine, 1895; Gluhbegovic, 1980). Analysis of fiber trajectories after anterograde tracer injections in the macaque (Schmahmann and Pandya, 2006; Lehman et al., 2011) indicate that fibers are indeed fasciculated over extended lengths in many cases but in other cases axonal trajectories may be distributed more diffusely. Another important issue that affects the accuracy of non-invasively reconstructed cortico-cortico connections is the angle at which fibers enter and leave cerebral cortex. Do fibers typically traverse the gray-white boundary approximately at right angles, as has been assumed (e.g., Tuch et al., 2003)? Or do they typically 'peel off' and traverse this boundary obliquely, as suggested by examination of myelinated axon trajectories (K. Dikranian, M. Glasser, D. Van Essen, unpublished observations)? Detailed analysis of such issues may provide improved, anatomically grounded constraints that can be used to better constrain the non-invasive reconstruction of long-distance pathways.

2.5 Functional connectivity and neurovascular coupling

Analyses of brain circuits have benefited greatly by the emergence of methods for inferring 'functional connectivity' using correlations in the fMRI BOLD signal (e.g., Smith et al, 2011). The fundamental underpinnings of this approach is that correlations in the low-frequency BOLD signal provide evidence for which brain regions are functionally coupled through direct or indirect anatomical connections (Biswal et al., 1995; Vincent et al., 2007). For such analyses, spatial resolution is limited not only by the voxel size used for data acquisition, but also by the spatial relationships associated with neurovascular coupling. In particular, in gradient echo (GRE) BOLD fMRI images (the most commonly used approach for functional brain imaging and to date the only approach successfully used for resting state fMRI) the functional signals are largest in draining vessels (Menon et al., 1993; Uludag et al., 2009) that, for cerebral cortex, lie on the pial surface. This is particularly true at magnetic fields of 1.5 – 4 Tesla (Duong et al., 2003). This is a serious problem for analyzing buried cortex, because larger vessels drain from both banks of a given sulcus and thus reflect neural activity of regions that reside in close proximity in space but may be widely separated in function. The confound can be reduced by restricting analysis to gray-matter voxels (e.g., Kolster et al., 2010), but it is not eliminated because the BOLD effect from blood vessels extends outside blood vessel boundaries by about the blood vessel diameter (up to ~1 mm; Ogawa et al., 1993)[1].

Of course, having strong signals of truly cortical origin will help. For ultrahigh magnetic fields of 7 Tesla (7T) and above, there is a stronger microvascular contribution from capillaries, small post-capillary venules, and small intracortical veins (Yacoub et al., 2005; Uludag et al., 2009). Mapping signals associated with this intracortical vasculature may be distinguishable in analysis methods such as independent component analysis (ICA) and segregated from contributions originating from the pial vessels based on their different spatio-temporal signatures given sufficient spatial and temporal resolution (De Martino et al., 2011). Laminar-specific analyses can also further improve spatial fidelity of the GRE BOLD functional signals at 7T, by excluding not only the pial surface but also superficial cortical layers as well to eliminate the extravascular BOLD effect from the surface veins extending over the cortex (Polimeni et al., 2010); however, this approach sacrifices

[1]The only exception is when the blood vessels run roughly parallel to the main magnetic field (approximately in the superior-inferior direction); in such regions, blood vessels do not have a significant extravascular BOLD effect (Ogawa et al., 1993)

information about the superficial layers, whose connections differ from those of deeper layers.

2.6. Individual variability

The nature and magnitude of individual variability is markedly different for each major brain structure. Variability is greatest for the cerebral cortex, where it involves large differences in the pattern of cortical convolutions, in the location of cortical areas relative to these convolutions, in the size of each area, and presumably also in the patterns of long-distance connectivity. Current methods used to compensate for individual variability involve registration to a standard atlas using volume-based or surface-based algorithms that are constrained by shape features. In general, surface-based registration outperforms volume-based registration (nonlinear or linear) in achieving good intersubject alignment (Fischl et al., 2008; Van Essen et al., 2011b). However, the quality of intersubject registration is variable and is worst in regions of high folding variability (Fig. 4). Approaches that capitalize on measures more closely related to cortical areas than folding patterns, e.g. connectivity data or cortical myelination (Glasser and Van Essen 2011), should in principle be able to achieve much better alignment.

3. Addressing the challenges

Given the neurobiological challenges posed in the preceding section, it is critical for future connectome efforts to obtain the best possible imaging data, because no amount of post-acquisition refinements can overcome the fundamental limitations imposed by the spatial resolution, sensitivity, and signal-to-noise at the front end of the process. For the MR-based modalities, this entails optimization of both the hardware and the pulse sequences used for data acquisition. For dMRI, this involves estimating the orientation of white matter fiber bundles as accurately as possible, especially in regions where multiple fiber bundles intersect one another at various angles or where a fiber bundle bends or fans out and splits into multiple bundles. Reducing voxel size and improving signal-to-noise are key. The issues involved in achieving these objectives differ for fMRI vs. dMRI and for 3T vs. ultrahigh fields (7T and higher).

3.1 Data acquisition at 3T

A number of refinements are expected to significantly improve the quality of fMRI and dMRI data relative to conventional 3T scanners and data acquisition methods. These include improved pulse sequences and hardware.

Short-TR pulse sequences—A major issue in acquiring whole-brain fMRI and dMRI at high spatial resolution is the acquisition times involved. For conventional pulse sequences, the repetition time (‘TR’, or time of full-volume coverage) equals the product of the number of volume slices and the acquisition period for each slice. This limits the temporal resolution desirable for fMRI and requires unduly long scan durations for high angular resolution dMRI, Both problems are exacerbated when aiming for higher spatial resolution. Techniques such as in-plane parallel imaging can reduce the image acquisition period for each slice, but only to a limited extent when a physiological contrast preparation period (e.g. for neuronal activity or water diffusion) precedes the spatial encoding period for each slice. Recently, significant shortening of TR (i.e., acceleration of volume coverage) for both fMRI and dMRI has been achieved using “slice” multiplexing, in which multiple slices are excited and acquired simultaneously, thus sharing a common contrast and spatial encoding periods. The UMinn group introduced this approach first for high-resolution whole brain fMRI at 7T (Moeller et al., 2008; 2010), benefitting from longstanding support for technology development in high and ultrahigh field imaging as an NCRR-funded Biotechnology

Research Center. Development of the slice-accelerated "Multiband" fMRI technique was driven by the need to avoid inordinately long acquisition times for very high-resolution, whole brain coverage that is feasible at 7T. Fortunately, the simultaneous slice strategy was tailor-made for the needs of the HCP at all field strengths. It has already been shown to significantly increase the statistical power in functional connectivity analyses (Feinberg et al, 2010) and reduce the acquisition time of diffusion data; therefore, it has become the core sequence design for both HCP consortia. Under HCP support, additional accelerations by combining the Multiband approach with the SIR technique (Feinberg et al., 2010) and improvements in unaliasing of simultaneously acquired slices (Setsompop et al., 2011) were introduced. The slice-accelerated techniques with additional, as yet unpublished, advances will be indispensible for the HCP and will be evaluated for achieving higher spatial and temporal resolution in fMRI and higher q-space coverage for dMRI. These pulse sequences and the image reconstruction software that operates within the scanner environment (ICE in Siemens parlance) can be used in standard Siemens 3T systems with 20 or 32-channel head coils and are available through the UMinn component of the WU-Minn HCP consortium; availability of the same capability on other platforms (GE, Phillips) is anticipated in 2013 or 2014.

3T scanners—Both the WU-Minn and MGH/UCLA consortia will use specialized 3T scanners designed to provide major advances in dMRI data acquisition. Both 3T scanners are based on the Siemens Skyra platform with a customized gradient insert and power amplifiers that will provide higher maximal gradient strengths. The WU-Minn 3T will attain at least 100 mT/m, compared to the 40 mT/m of a standard 3T scanner. Because it combines existing hardware components adapted from other systems, the WU-Minn connectome scanner was configured to provide the reliable performance that is essential for scanning the targeted number of 1200 healthy adults over a 3 year period (Van Essen et al., 2011). The MGH-based connectome scanner employs a more ambitious design that attains a maximum gradient strength of 300 mT/m using new hardware and tradeoffs in gradient linearity.

The theoretical benefit of increased gradient strength for dMRI follows a highly nonlinear relationship that depends upon the diffusion weighting imposed; the parameter b is a useful measure of this weighting[2]. Diffusion encoding, especially for large b values, typically takes 100 to 150 ms using conventional gradients. Since this diffusion encoding occurs during T2 decay, significant signal-to-noise (SNR) loss occurs in the process. As maximum gradient strength increases, diffusion encoding time can be reduced and SNR improved. Figure 5 illustrates percent SNR (relative to that attainable at 300 mT/m) when the maximum gradient strength is used to attain the shortest possible echo time (TE) in a monopolar diffusion encoding scheme. Under reasonable assumptions and for b values of less than 10^4 s/mm^2, the SNR benefit for 100 mT/m is expected to be 50% to 100% better than a conventional scanner and ~70 - 80% of that for 300 mT/m (see Figure 5; see also Fig. 2 in Van Essen et al., 2011). Thus, both the WU-Minn and MGH HCP scanners will achieve significant improvements over standard 3T scanners due to the increased gradient strength. In both consortia, the slew rates will be limited by peripheral and cardiac thresholds for in vivo imaging and will not be faster than the conventional scanners.

The Skyra has improved electronics that yields better SNR than older Siemens systems. In addition, both WU-Minn and MGH/UCLA Skyra systems are capable of handling up to 64 receive channels, though Siemens currently offers only a 32 channel receive coil. Accelerated sequences that rely on spatial sensitivities of array coils to unalias images, as

[2]For two gradient pulses of duration δ separated by interval Δ, i.e. the so called monopolar or Stejskal-Tanner diffusion weighting (Stejskal and Tanner 1965), and for gradient pulses with instantaneous rise and decay times, the b value is given by $b = (\gamma \cdots G \cdots \delta)^2(\Delta - \delta/3)$, where G is the gradient amplitude and γ is the gyromagnetic ratio of the nucleus used in the MR experiment.

will be employed in HCP, will likely benefit from advanced head coils having 48 to 64 elements currently being designed at UMinn, and at MGH.

3.2 Data acquisition at ultrahigh fields

While major improvements in fMRI and dMRI data acquisition can be achieved using 3T scanners, the rapidly evolving arena of ultrahigh field MR scanning opens additional exciting opportunities. The WU-Minn consortium plans to scan 200 subjects (a subset of the 1,200 scanned at 3T at WashU) using a 7T scanner at UMinn. The 7T system, while less mature and more challenging to work with than the 3T scanner, offers major advantages for the resting and task-based fMRI studies, and potentially also for diffusion-based techniques if sufficiently short echo times can be achieved for diffusion weighting. In addition, a new 10.5T scanner is currently under development at UMinn via a separately funded grant. Some HCP subjects will be scanned at 10.5T if it becomes operational in time. In any event it is important to anticipate how this higher field strength will serve connectomic studies in the future.

For all of the MRI approaches to be used in the HCP, a key parameter is spatial resolution. This is ultimately determined by the available SNR, since the minimum voxel volume achievable is directly related to SNR. For fMRI studies, another critical issue is the spatial fidelity of the BOLD signal relative to neuronal activity, which improves with increasing magnetic field. At low fields, BOLD signals originate mainly from large draining vessels. When acquired at high resolution, vessels on the pial surface are clearly discernible, as in venograms (Segebarth et al., 1994; Hoogenraad et al., 1999). At ultrahigh fields, this large vessel contribution persists in GRE fMRI images, but the contribution of the microvasculature increases supra-linearly with magnetic field and is also robustly detectable (Ugurbil et al, 2003).

Another potential gain at 7T may come from using spin-echo (SE) BOLD pulse sequences rather than GRE BOLD in order to enhance microvascular and suppress macrovascular contributions (Duong et al., 2003; Yacoub et al., 2003; Uludag et al., 2009). This approach can reveal robust signals for task based functional mapping at 7T (Yacoub et al., 2007; 2008), approximately comparable to what is obtained at 3T with conventional GRE BOLD. SE BOLD, however, does not have the spatial accuracy at lower fields such as 3T owing to persisting intravascular blood T2 changes coupled to alterations in neuronal activity (Norris et al., 2002; Duong et al., 2003). Nor does it have the sensitivity to yield robust resting state fMRI maps even at 7T (Yacoub et al., unpublished observations) where the temporal inefficiencies (due to RF power deposition limits) of SE imaging limit whole brain acquisitions.

The increased spatial fidelity achieved at ultrahigh fields and sequences like (SE) EPI and 3D GRASE, combined with the field-dependent gains in SNR has allowed functional mapping at the level of cortical columns, including orientation domains (Yacoub 2007, 2008) and axis of motion features in MT with laminar differentiation (Zimmermann et al., 2011). These capabilities have yet to be extensively used in cognitive neuroscience, in part because of the challenge in achieving high resolution over the whole brain. However, engineering and methodological advances over the last decade now enable the acquisition of excellent, high resolution (mm or submillimeter isotropic) whole brain images at 7T, at least with the GRE approach. For example, a whole-brain analysis of resting state networks at 1 mm isotropic resolution (De Martino et al., 2011) revealed signals primarily within cortical gray matter, reducing the problem of cross-talk between opposite banks of sulci (Section 2.5). Increasing the number of channels for the RF coils (e.g., to 48 to 64 channels) combined with better 7T electronics should lead to further improvements in SNR.

Additional gains are expected at 10.5T in image SNR (Vaughan et al., 2001) and accuracy of mapping signals due to further improvements in the microvascular contribution (Uludag et al., 2009). Like 7T, 10.5T has the potential to shine for high resolution resting and task based fMRI. However, the technical challenges to be faced at 10.5T should not be underestimated, given the experience with existing 9.4T scanners. At UMinn, the 9.4T system has been abandoned as an fMRI scanner because gradients compatible with the "head-only" 65 cm bore space have failed to tolerate EPI type sequences. However, 9.4T has been a great learning experience from which the 10.5T has and will continue to benefit. Provided the magnet meets technical specifications, as is likely, given the record of the manufacturer (Agilent), we are optimistic that the new 10.5T scanner will avoid the difficulties encountered at 9.4T and will provide resting-state and task fMRI data that will permit analysis at the level of cortical layers and columns. Besides the many technical challenges with data acquisition, there will be additional challenges in dealing with the incredibly large amount of data to be generated at high resolution with highly parallel and highly accelerated acquisitions.

dMRI at 7T—There is a common misconception that ultrahigh fields do not provide a benefit in SNR for dMRI. However, the theoretical curves in Figure 6 illustrate that there are potentially large SNR gains for 7T provided that short echo times (TE) can be attained. At ultrahigh fields, the T2 gets shorter; hence diffusion encoding produces a larger SNR loss for a given TE. At the lowest possible value (TE near 0), the ultrahigh fields provide slightly better than linear (with field magnitude) SNR gain without considering T1 effects. As TE increases, the 7T advantage compared to 3T declines, then reverses. Thus, the TE that can be achieved at the 7T instrument for diffusion encoding becomes critical. At echo times typical of most dMRI experiments, (e.g. ~150 ms), 7T indeed does not provide much of an advantage (Fig. 6). But TE's of ~50 ms that may be attainable using increased maximum gradients strengths would yield significant gains at 7T as compared to 3T. The simulations in Figure 6 depend on T2 values for brain tissue, for which there is not a consensus (see Fig. legend). If the white matter T2 is assumed to be 70 ms at 3T, the upper limit of values reported previously, then the 7T advantages start at te_{k1} ~75 ms as opposed to ~150 ms. Irrespective of the details, the key point is that, all else being equal, 7T will be advantageous for dMRI if TE for diffusion encoding can be kept sufficiently short.

Similar considerations apply to dMRI acquisition at 10.5T. Intrinsic SNR, without T1 and T2 effects, will increase at 10.5T relative to 7T approximately linearly. However, T2 will be shorter and T1 somewhat longer, though the latter will not be a significant contributor for the TR range likely to be used for dMRI (≳2 sec), as shown for 7T vs. 3T (Figure 6). The challenge will be to reduce TE below ~50 ms. The TE in dMRI sequences depends on the maximum gradient amplitude available. Currently, 80 mT/m is available for 7T using head gradients, which also allows faster slew rates (~400 mT/m/ms) while avoiding peripheral nerve and cardiac stimulation limits encountered using body gradients. These gradients can attain TE of ~50 ms for monopolar diffusion weighting for b~3000 s/mm^2. Both at 7T and in particular at 10.5T, stimulated echo (STE) sequences will be worth exploring. These sequences have an intrinsic SNR loss of factor 2, and, as such, are not suitable for 3T; but they can achieve very large b values without a prolonged echo time during which the signal is decaying with time constant T2. Because the intrinsic SNR increases with field magnitude, the two-fold SNR loss in the STE sequences will be approximately a wash at 7T relative to 3T and will leave 10.5T with an SNR gain relative to 3T at TE~0. But when diffusion encoding is imposed, the same b value will be attained with much shorter TE in the STE sequence than in the spin-echo version that must be used at 3T, which will give an SNR advantage to the STE at ultrahigh fields compared to SE at 3T. The longer T1s at the 7T and 10.5T will also be an advantage for the STE sequence that makes this approach potentially attractive at very high fields. Of course, ideally one would not wish to sacrifice SNR at all

and aim for very high maximum gradients that are usable with spin-echoes at ultrahigh fields. An ambitious but theoretically achievable scenario for dMRI would include a head gradient that could achieve perhaps ≳150 mT/m, perhaps even ~300 mT/m, with slew rates of ≳400 mT/m/ms operating for both 7T and 10.5T. Unfortunately, there is no such engineering project at the present, but one can dream of this as a future development.

MRI-savvy colleagues will immediately think of important details that impact the SNR arguments presented here. For example, extreme in-plane acceleration is needed in order to obtain EPI images without signal dropouts or large distortions at very high fields. There is a consequent SNR loss with such accelerations. On the other hand, the shorter TE to the central echo point will enhance SNR. Faster rapid signal decay at the higher magnetic fields during an EPI readout train will lead to some effective SNR loss and increase in the image point-spread function, etc. With any particular set of experimental parameters, accounting for all of these effects is straightforward. Here, however, we have intentionally avoided extensive simulations. The general message nevertheless remains valid: dMRI can perform well at increasing fields if TE can be made appropriately short. This is a challenge but likely to be feasible in the long run.

3.3. Other data modalities and analyses

In this article, we have concentrated on R-fMRI and dMRI data acquisition because these domains are fundamentally the most rate-limiting for estimating human brain connectivity *in vivo* and for addressing the neurobiological challenges outlined in Section 2. However, R-fMRI and dMRI data acquisition are entry points to a much broader effort that is essential to a better understanding of the human connectome. The wider effort includes many levels of data analysis and visualization as well as cross-modal integration with other important modalities based on imaging, behavior, and genetics. For the WU-Minn HCP consortium, this includes task-fMRI to be carried out on all 1,200 subjects and MEG/EEG on 100 subjects. Extensive behavioral assessments will be carried out in all subjects. Moreover, blood sample collection will allow genotyping in year 5 of the grant, likely including whole genome sequencing. Together, this will provide a dataset of unprecedented richness for exploring the relationships between brain connectivity and behavioral phenotypes as well as genetic underpinnings. The subjects will be 300 twin pairs and 600 non-twin siblings, which will allow exploration of the heritability of brain connections and will enhance the statistical power of the genetic analyses. This is described in greater detail elsewhere (Van Essen et al., 2011c).

The data analysis efforts for the HCP will span a broad range of efforts that we can only briefly touch upon here. Of particular import are efforts to address (i) the brain parcellation problem, (ii) intersubject variability and correlating connectivity with other phenotypes, and (iii) providing an informatics and visualization platform that will enable a new type of discovery science through powerful data mining capabilities (Marcus et al., 2011). These methods and approaches are under active development and will be considered further in future publications.

3.4. The human connectome in a decade

Funding for the current WU-Minn HCP will conclude in 2015, but the ConnectomeDB database will be maintained at Washington University for an additional 5 years. How will our understanding of the human connectome expand and evolve over the coming decade? Will the advances be incremental, or can we anticipate transformative neurobiological insights to emerge? Before speculating briefly on these issues, it is instructive to consider the Human Genome Project, launched in 1990 and concluded in 2003 at a cost of ~3 billion dollars, two orders of magnitude greater than the current HCP investment. The genome

sequencing effort has been extraordinarily successful, including many ways that were not anticipated in its early days. It has led to deep and surprising insights into fundamental aspects of genome organization and function, enabled numerous medical advances, and powered new biotechnology industries.

Among the many differences between human brain macro-connectomics and genome sequencing is the fidelity with which data are acquired and analyzed. Genome sequencing is extremely accurate (99.99% or better), making it feasible to distinguish differences between individuals at the single nucleotide level. However, this is coupled with a very low level of nucleotide diversity across individuals -- only about 1 part in 1,000. The accuracy with which human brain connectivity can be quantitatively assessed is vastly inferior to genome sequencing. On the other hand, the degree of individual variability in connectivity patterns is likely to be far greater. Each cortical area varies in surface area by two-fold or more across individuals (Van Essen et al., 2011b) and the strength of pathways between a pair of cortical areas can vary by one or two orders of magnitude (Markov et al., 2011). Until the HCP data are acquired and analyzed, we simply will not know what sensitivity and reliability to expect in comparing connectomes across individuals and relating connectivity to behavioral phenotypes and genetic differences. Despite these caveats, we are optimistic that major insights will emerge from mining of HCP data. In broad strokes, this will include (i) a far more accurate charting of brain parcellations (particularly neocortical and cerebellar parcels), brain networks, and their dynamics; (ii) a quantitative characterization of network variability across individuals; and (iii) correlations between behavioral phenotypes and brain networks that provide a deeper understanding of the neural basis of individual variability. Such insights might be related to working memory, perceptual categorization, emotion, personality, or any of the many other phenotypes that will be available for data mining.

Our focus in this article has been on the healthy adult human brain, based on the mandate from NIH to the HCP. However, the dramatic changes in brain circuits that occur during development and aging will be amenable to analysis using the approaches described here. Even more important in the long run will be the advances in understanding the neurobiological bases of brain diseases and disorders that afflict hundreds of millions of individuals worldwide and extract an extraordinary toll in terms of human suffering and economic impact. The prospect of providing improvements in diagnosis and treatment of brain disorders by capitalizing on a broad spectrum of methodological advances provides ample motivation for continued investment in human connectomics.

4. Concluding remarks

Charting the structure, function, connectivity, and development of the human brain (brain cartography, broadly writ) is one of the great challenges of the 21st century, just as cartography of the earth's surface was the domain of intrepid explorers earlier this millennium. There are interesting high-level similarities in the types of technological evolution for both types of cartography. The past millennium has seen four major revolutions in cartography of the earth's surface (Fig. 7, left). The first period involved many centuries of colorful but initially very rudimentary maps revealed by early explorers. During most of the 20th century, book atlases of increasing thickness emerged as a way to represent the increasing amount and type of information that could be encoded in maps. In the latter part of the century, satellite imagery opened up a vast new realm of digital information that could be acquired using high-resolution satellite-based photography. In the 21st century, cartography made another radical advance that was powered not just by improved spatial resolution but by the highly interactive nature of navigation afforded by Google Earth and its conspecific applications.

In roughly analogous fashion, four major revolutions in cartography of the human brain can be discerned over the past century (Fig. 7, right). The first period involved classical maps of brain architecture and functional organization provided by Brodmann and other anatomists. The second period involved brain atlases represented in books, particularly the well-known Talairach atlas (Talairach and Tournoux, 1988). The third period involved maps of brain structure and function acquired using MR-based methods and visualization of brain volumes and surfaces. Now, in the 21st century, neuroscience is entering a new realm in which human brain connectivity can be analyzed using the powerful tools discussed above and visualized using increasingly sophisticated navigational and informatics tools. It is likely that some of the tools available for a '2020' view of the human brain will far outstrip the limits of our current imagination, just as Google Maps were not even a glimmer in anyone's eye a decade or two ago.

Acknowledgments

We thank M. Glasser, S. Curtiss, S. Smith, O. Sporns, D. Feinberg, E. Yacoub, and S. Petersen for comments on the manuscript and our many other colleagues in the WU-Minn HCP consortium for invaluable discussions over the past two years that have helped frame the issues and advance our thinking about the opportunities and challenges in human connectomics. Supported by the Human Connectome Project (1U54MH091657-01) from the 16 NIH Institutes and Centers that Support the NIH Blueprint for Neuroscience Research, by NIMH grant R01 MH 60974 (DVE) and National Center for Research Resources (NCRR) grant P41 RR008079 (KU).

References

Akil H, Martone ME, Van Essen DC. Challenges and opportunities in mining neuroscience data. Science. 2011; 331:708–712. [PubMed: 21311009]

Amunts K, Lenzen M, Friederici A, Schleicher A, Morosan P, Palomero-Gallagher N, Zilles K. Broca's Region: Novel Organizational Principles and Multiple Receptor Mapping. PLoS biology. 2010; 8:330–357.

Azevedo FA, Carvalho LR, Grinberg LT, Farfel JM, Ferretti RE, Leite RE, Jacob Filho W, Lent R, Herculano-Houzel S. Equal numbers of neuronal and nonneuronal cells make the human brain an isometrically scaled-up primate brain. The Journal of comparative neurology. 2009; 513:532–541. [PubMed: 19226510]

Baizer JS, Ungerleider LG, Desimone R. Organization of visual inputs to the inferior temporal and posterior parietal cortex in macaques. J Neurosci. 1991; 11:168–190. [PubMed: 1702462]

Beckmann CF, DeLuca M, Devlin JT, Smith SM. Investigations into resting-state connectivity using independent component analysis. Philosophical transactions of the Royal Society of London. 2005; 360:1001–1013. [PubMed: 16087444]

Behrens TE, Sporns O. Human connectomics. Current opinion in neurobiology. 2011

Biswal B, Yetkin FZ, Haughton VM, Hyde JS. Functional connectivity in the motor cortex of resting human brain using echo-planar MRI. Magn Reson Med. 1995; 34:537–541. [PubMed: 8524021]

Bock DD, Lee W-CA, Kerlin A, ML A, G H, AW W, S Y, ER S. Network anatomy and in vivo physiology of visual cortical neurons. Nature. 2011; 471:177–182. [PubMed: 21390124]

Briggman KL, Helmstaedter M, Denk W. Wiring specificity in the direction-selectivity circuit of the retina. Nature. 2011; 471:183–188. [PubMed: 21390125]

Buckner RL, Krienen FM, Castellanos A, Diaz JC, Yeo BT. The Organization of the Human Cerebellum Estimated By Intrinsic Functional Connectivity. J Neurophysiol. 2011

Cohen AL, Fair DA, Dosenbach NU, Miezin FM, Dierker D, Van Essen DC, Schlaggar BL, Petersen SE. Defining functional areas in individual human brains using resting functional connectivity MRI. NeuroImage. 2008; 41:45–57. [PubMed: 18367410]

Collins CE, Airey DC, Young NA, Leitch DB, Kaas JH. Neuron densities vary across and within cortical areas in primates. Proceedings of the National Academy of Sciences of the United States of America. 2010; 107:15927–15932. [PubMed: 20798050]

Crick F, Jones E. Backwardness of human neuroanatomy. Nature. 1993; 361:109–110. [PubMed: 8421513]

De Martino F, Esposito F, van de Moortele PF, Harel N, Formisano E, Goebel R, Ugurbil K, Yacoub E. Whole brain high-resolution functional imaging at ultrahigh magnetic fields: an application to the analysis of resting state networks. NeuroImage. 2010; 57:1031–1044. [PubMed: 21600293]

Dejerine, J. Anatomie des Centres Nerveux. Rueff et Cie; Paris: 1895.

DeYoe EA, Van Essen DC. Segregation of efferent connections and receptive field properties in visual area V2 of the macaque. Nature. 1985; 317:58–61. [PubMed: 2412132]

DeYoe EA, Felleman DJ, Van Essen DC, McClendon E. Multiple processing streams in occipitotemporal visual cortex. Nature. 1994; 371:151–154. [PubMed: 8072543]

Duong TQ, Yacoub E, Adriany G, Hu X, Ugurbil K, Kim SG. Microvascular BOLD contribution at 4 and 7 T in the human brain: gradient-echo and spin-echo fMRI with suppression of blood effects. Magn Reson Med. 2003; 49:1019–1027. [PubMed: 12768579]

Feinberg DA, Reese TG, Wedeen VJ. Simultaneous echo refocusing in EPI. Magn Reson Med. 2002; 48:1–5. [PubMed: 12111925]

Feinberg DA, Moeller S, Smith SM, Auerbach E, Ramanna S, Glasser MF, Miller KL, Ugurbil K, Yacoub E. Multiplexed Echo Planar Imaging for Sub-Second Whole Brain FMRI and Fast Diffusion Imaging. PLoS One. 2010; 5:e15710. [PubMed: 21187930]

Felleman DJ, Van Essen DC. Distributed hierarchical processing in the primate cerebral cortex. Cereb Cortex. 1991; 1:1–47. [PubMed: 1822724]

Fischl B, Rajendran N, Busa E, Augustinack J, Hinds O, Yeo BT, Mohlberg H, Amunts K, Zilles K. Cortical folding patterns and predicting cytoarchitecture. Cereb Cortex. 2008; 18:1973–1980. [PubMed: 18079129]

Fox MD, Raichle ME. Spontaneous fluctuations in brain activity observed with functional magnetic resonance imaging. Nature reviews. 2007; 8:700–711.

Gerbella M, Belmalih A, Borra E, Rozzi S, Luppino G. Cortical connections of the macaque caudal ventrolateral prefrontal areas 45A and 45B. Cereb Cortex. 2010; 20:141–168. [PubMed: 19406905]

Gerbella M, Belmalih A, Borra E, Rozzi S, Luppino G. Cortical connections of the anterior (F5a) subdivision of the macaque ventral premotor area F5. Brain structure & function. 2011; 216:43–65. [PubMed: 21132509]

Glasser MF, Van Essen DC. Myelin content as revealed by T1- and T2-weighted MRI. J Neuroscience. 2011; 31:11597–11616.

Gluhbegovic N. The Human Brain: A Photographic Guide. Harpercollins. 1980:176.

Hagmann P, Cammoun L, Gigandet X, Meuli R, Honey CJ, Wedeen VJ, Sporns O. Mapping the structural core of human cerebral cortex. PLoS biology. 2008; 6:e159. [PubMed: 18597554]

He SQ, Dum RP, Strick PL. Topographic organization of corticospinal projections from the frontal lobe: motor areas on the lateral surface of the hemisphere. J Neurosci. 1993; 13:952–980. [PubMed: 7680069]

He SQ, Dum RP, Strick PL. Topographic organization of corticospinal projections from the frontal lobe: motor areas on the medial surface of the hemisphere. J Neurosci. 1995; 15:3284–3306. [PubMed: 7538558]

Hoogenraad FG, Hofman MB, Pouwels PJ, Reichenbach JR, Rombouts SA, Haacke EM. Sub-millimeter fMRI at 1.5 Tesla: correlation of high resolution with low resolution measurements. J Magn Reson Imaging. 1999; 9:475–482. [PubMed: 10194720]

Iturria-Medina Y, Sotero RC, Canales-Rodriguez EJ, Aleman-Gomez Y, Melie-Garcia L. Studying the human brain anatomical network via diffusion-weighted MRI and Graph Theory. NeuroImage. 2008; 40:1064–1076. [PubMed: 18272400]

Jones DK, Cercignani M. Twenty-five pitfalls in the analysis of diffusion MRI data. NMR in biomedicine. 2010; 23:803–820. [PubMed: 20886566]

Kolster H, Peeters R, Orban GA. The retinotopic organization of the human middle temporal area MT/V5 and its cortical neighbors. J Neurosci. 2010; 30:9801–9820. [PubMed: 20660263]

Lehman JF, Greenberg BD, McIntyre CC, Rasmussen SA, Haber SN. Rules ventral prefrontal cortical axons use to reach their targets: implications for diffusion tensor imaging tractography and deep brain stimulation for psychiatric illness. J Neurosci. 2011; 31:10392–10402. [PubMed: 21753016]

Lewis JW, Van Essen DC. Mapping of architectonic subdivisions in the macaque monkey, with emphasis on parieto-occipital cortex. The Journal of comparative neurology. 2000; 428:79–111. [PubMed: 11058226]

Lichtman JW, Sanes JR. Ome sweet ome: what can the genome tell us about the connectome? Current opinion in neurobiology. 2008; 18:346–353. [PubMed: 18801435]

Livingstone MS, Hubel DH. Specificity of intrinsic connections in primate primary visual cortex. J Neurosci. 1984; 4:2830–2835. [PubMed: 6209365]

Mai, J.; Paxinos, G. The Human Nervous System. 3rd edition. Academic press; 2011. p. 1428

Marcus DS, Harwell J, Olsen T, Hodge M, Glasser MF, Prior F, Jenkinson M, Laumann T, Curtiss SW, Van Essen DC. Informatics and data mining tools and strategies for the human connectome project. Frontiers in neuroinformatics. 2011; 5:4. [PubMed: 21743807]

Markov NT, Misery P, Falchier A, Lamy C, Vezoli J, Quilodran R, Gariel MA, Giroud P, Ercsey-Ravasz M, Pilaz LJ, Huissoud C, Barone P, Dehay C, Toroczkai Z, Van Essen DC, Kennedy H, Knoblauch K. Weight consistency specifies regularities of macaque cortical networks. Cereb Cortex. 2011; 21:1254–1272. [PubMed: 21045004]

Mars RB, Jbabdi S, Sallet J, O'Reilly JX, Croxson PL, Olivier E, Noonan MP, Bergmann C, Mitchell AS, Baxter MG, Behrens TE, Johansen-Berg H, Tomassini V, Miller KL, Rushworth MF. Diffusion-weighted imaging tractography-based parcellation of the human parietal cortex and comparison with human and macaque resting-state functional connectivity. J Neurosci. 2011; 31:4087–4100. [PubMed: 21411650]

Menon RS, Ogawa S, Tank DW, Ugurbil K. Tesla gradient recalled echo characteristics of photic stimulation-induced signal changes in the human primary visual cortex. Magn Reson Med. 1993; 30:380–386. [PubMed: 8412612]

Mitra PP, Thompson DJ, Ogawa S, Hu X, Ugurbil K. Spatio-temporal patterns in fMRI dat revealed by principal component analysis and subsequent low pass filtering. Proc Int Mag Reson Med. 1995; 2:817.

Moeller S, Auerbach E, Van de Moortele P-F, Adriany G, Ugurbil K. fMRI with 16 fold reduction using multibanded multislice sampling. Proc Int Soc Mag Reson Med. 2008; 16

Moeller S, Yacoub E, Olman CA, Auerbach E, Strupp J, Harel N, Ugurbil K. Multiband multislice GE-EPI at 7 tesla, with 16-fold acceleration using partial parallel imaging with application to high spatial and temporal whole-brain fMRI. Magn Reson Med. 2010; 63:1144–1153. [PubMed: 20432285]

Nelson SM, Cohen AL, Power JD, Wig GS, Miezin FM, Wheeler ME, Velanova K, Donaldson DI, Phillips JS, Schlaggar BL, Petersen SE. A parcellation scheme for human left lateral parietal cortex. Neuron. 2010; 67:156–170. [PubMed: 20624599]

Norris DG, Zysset S, Mildner T, Wiggins CJ. An investigation of the value of spin-echo-based fMRI using a Stroop color-word matching task and EPI at 3 T. NeuroImage. 2002; 15:719–726. [PubMed: 11848715]

Ogawa S, Tank DW, Menon R, Ellermann JM, Kim SG, Merkle H, Ugurbil K. Intrinsic signal changes accompanying sensory stimulation: functional brain mapping with magnetic resonance imaging. Proceedings of the National Academy of Sciences of the United States of America. 1992; 89:5951–5955. [PubMed: 1631079]

Ogawa S, Menon RS, Tank DW, Kim SG, Merkle H, Ellermann JM, Ugurbil K. Functional brain mapping by blood oxygenation level-dependent contrast magnetic resonance imaging. A comparison of signal characteristics with a biophysical model. Biophysical journal. 1993; 64:803–812. [PubMed: 8386018]

Pakkenberg B, Pelvig D, Marner L, Bundgaard MJ, Gundersen HJ, Nyengaard JR, Regeur L. Aging and the human neocortex. Exp Gerontol. 2003; 38:95–99. [PubMed: 12543266]

Polimeni JR, Fischl B, Greve DN, Wald LL. Laminar analysis of 7T BOLD using an imposed spatial activation pattern in human V1. NeuroImage. 2010; 52:1334–1346. [PubMed: 20460157]

Power JD, Cohen AL, Nelson SM, Wig GS, Barnes KA, Church JA, Vogel AC, Laumann TO, Miezin FM, Schlaggar BL, Petersen SE. Functional network organization of the human brain. Neuron. 2011 (in press).

Rooney WD, Johnson G, Li X, Cohen ER, Kim SG, Ugurbil K, Springer CS Jr. Magnetic field and tissue dependencies of human brain longitudinal 1H2O relaxation in vivo. Magn Reson Med. 2007; 57:308–318. [PubMed: 17260370]

Schmahmann, JD.; Pandya, DN. Fiber Pathways in the Brain. Oxford Univ Press; NY: 2006. p. 643

Segebarth C, Belle V, Delon C, Massarelli R, Decety J, Le Bas JF, Decorps M, Benabid AL. Functional MRI of the human brain: predominance of signals from extracerebral veins. Neuroreport. 1994; 5:813–816. [PubMed: 8018855]

Setsompop K, Gagoski BA, Polimeni JR, Witzel T, Wedeen VJ, Wald LL. Blipped-controlled aliasing in parallel imaging for simultaneous multislice echo planer imaging with reduced g-factor penalty. Magn Reson Med. 2011

Sincich LC, Jocson CM, Horton JC. V1 interpatch projections to v2 thick stripes and pale stripes. J Neurosci. 2010; 30:6963–6974. [PubMed: 20484638]

Smith SM, Miller KL, Salimi-Khorshidi G, Webster M, Beckmann CF, Nichols TE, Ramsey JD, Woolrich MW. Network modelling methods for FMRI. NeuroImage. 2011; 54:875–891. [PubMed: 20817103]

Sporns O, Tononi G, Kotter R. The human connectome: A structural description of the human brain. PLoS computational biology. 2005; 1:e42. [PubMed: 16201007]

Stanisz GJ, Odrobina EE, Pun J, Escaravage M, Graham SJ, Bronskill MJ, Henkelman RM. T1, T2 relaxation and magnetization transfer in tissue at 3T. Magn Reson Med. 2005; 54:507–512. [PubMed: 16086319]

Stejskal EO, Tanner JE. Spin diffusion measurements: spin-echoes in the presence of time dependent field gradient. J Chem Phys. 1965; 42:288–292.

Strick PL, Dum RP, Fiez JA. Cerebellum and nonmotor function. Annual review of neuroscience. 2009; 32:413–434.

Sultan F, Braitenberg V. Shapes and sizes of different mammalian cerebella. A study in quantitative comparative neuroanatomy. Journal fur Hirnforschung. 1993; 34:79–92. [PubMed: 8376757]

Talairach, J.; Tournoux, P. Coplanar Stereotaxic Atlas of the Human Brain. Thieme Medical; New York: 1988.

Tank DW, Ogawa S, Ugurbil K. Mapping the brain with MRI. Curr Biol. 1992; 2:525–528. [PubMed: 15336045]

Tuch DS, Reese TG, Wiegell MR, Wedeen VJ. Diffusion MRI of complex neural architecture. Neuron. 2003; 40:885–895. [PubMed: 14659088]

Ugurbil K, Adriany G, Andersen P, Chen W, Garwood M, Gruetter R, Henry PG, Kim SG, Lieu H, Tkac I, Vaughan T, Van De Moortele PF, Yacoub E, Zhu XH. Ultrahigh field magnetic resonance imaging and spectroscopy. Magn Reson Imaging. 2003; 21:1263–1281. [PubMed: 14725934]

Uludag K, Muller-Bierl B, Ugurbil K. An integrative model for neuronal activity-induced signal changes for gradient and spin echo functional imaging. NeuroImage. 2009; 48:150–165. [PubMed: 19481163]

van den Heuvel MP, Stam CJ, Kahn RS, Hulshoff Pol HE. Efficiency of functional brain networks and intellectual performance. J Neurosci. 2009; 29:7619–7624. [PubMed: 19515930]

Van Essen DC, et al. The Human Connectome Project: A data acquisition perspective. Neuroimage. 2001c (in revision).

Van Essen DC, Glasser MF, Dierker D, Harwell J. Cortical parcellations of the Macaque monkey analyzed on surface-based atlases. 2011a Cereb Cortex 2 Nov epub ahead of print 10.1093/cercor/bhr290.

Van Essen DC, Glasser MF, Dierker D, Harwell J, Coalson T. Parcellations and hemispheric asymmetries of human cerebral cortex analyzed on surface-based atlases. 2011b Cereb Cortex 2 Nov epub ahead of print 10.1093/cercor/bhr291.

Vaughan JT, Garwood M, Collins CM, Liu W, DelaBarre L, Adriany G, Andersen P, Merkle H, Goebel R, Smith MB, Ugurbil K. 7T vs. 4T: RF power, homogeneity, and signal-to-noise comparison in head images. Magn Reson Med. 2001; 46:24–30. [PubMed: 11443707]

Vincent JL, Patel GH, Fox MD, Snyder AZ, Baker JT, Van Essen DC, Zempel JM, Snyder LH, Corbetta M, Raichle ME. Intrinsic functional architecture in the anaesthetized monkey brain. Nature. 2007; 447:83–86. [PubMed: 17476267]

Wansapura JP, Holland SK, Dunn RS, Ball WS Jr. NMR relaxation times in the human brain at 3.0 tesla. J Magn Reson Imaging. 1999; 9:531–538. [PubMed: 10232510]

Wig GS, Schlaggar BL, Petersen SE. Concepts and principles in the analysis of brain networks. Annals of the New York Academy of Sciences. 2011; 1224:126–146. [PubMed: 21486299]

Yacoub E, Harel N, Ugurbil K. High-field fMRI unveils orientation columns in humans. Proceedings of the National Academy of Sciences of the United States of America. 2008; 105:10607–10612. [PubMed: 18641121]

Yacoub E, Van De Moortele PF, Shmuel A, Ugurbil K. Signal and noise characteristics of Hahn SE and GE BOLD fMRI at 7 T in humans. NeuroImage. 2005; 24:738–750. [PubMed: 15652309]

Yacoub E, Shmuel A, Logothetis N, Ugurbil K. Robust detection of ocular dominance columns in humans using Hahn Spin Echo BOLD functional MRI at 7 Tesla. NeuroImage. 2007; 37:1161–1177. [PubMed: 17702606]

Yacoub E, Duong TQ, Van De Moortele PF, Lindquist M, Adriany G, Kim SG, Ugurbil K, Hu X. Spin-echo fMRI in humans using high spatial resolutions and high magnetic fields. Magn Reson Med. 2003; 49:655–664. [PubMed: 12652536]

Yeo BT, Krienen FM, Sepulcre J, Sabuncu MR, Lashkari D, Hollinshead M, Roffman JL, Smoller JW, Zollei L, Polimeni JR, Fischl B, Liu H, Buckner RL. The organization of the human cerebral cortex estimated by intrinsic functional connectivity. J Neurophysiol. 2011; 106:1125–1165. [PubMed: 21653723]

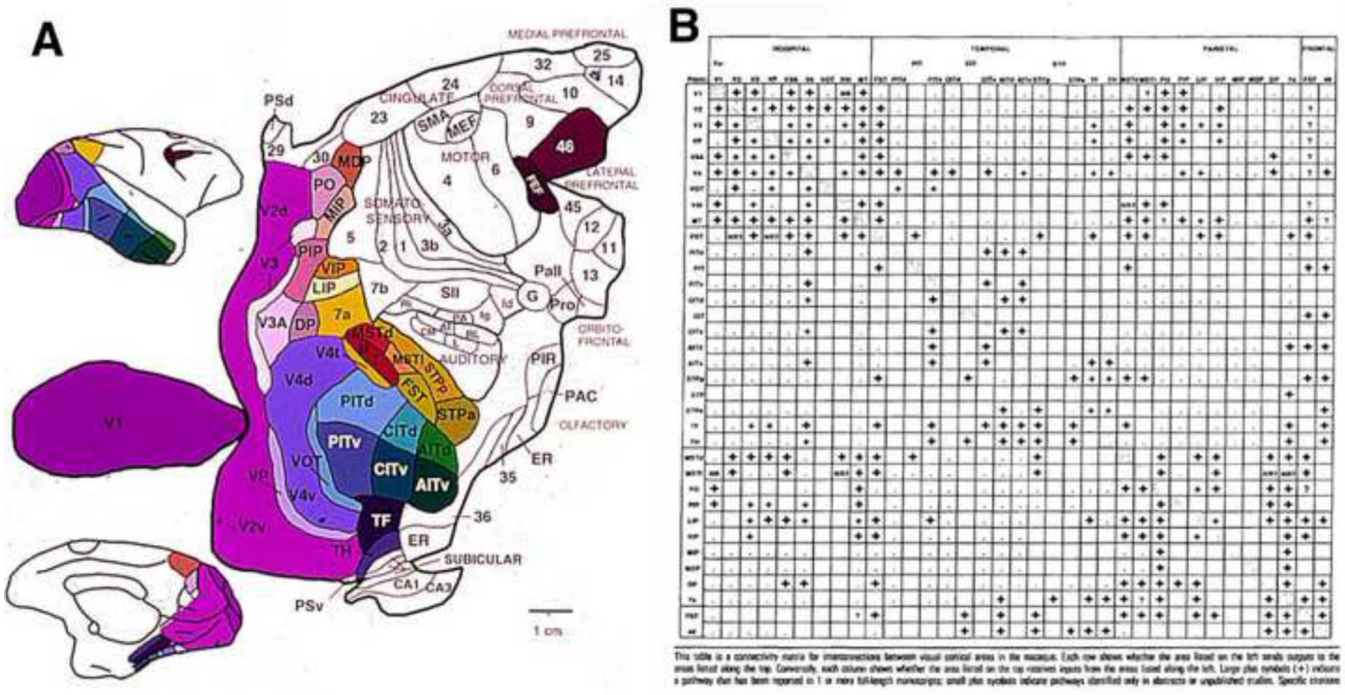

Figure 1.

A. A flat map of cortical areas in the macaque. B. A 32 × 32 binary connectivity matrix for macaque visual areas. Reproduced, with permission, from Felleman & Van Essen (1991).

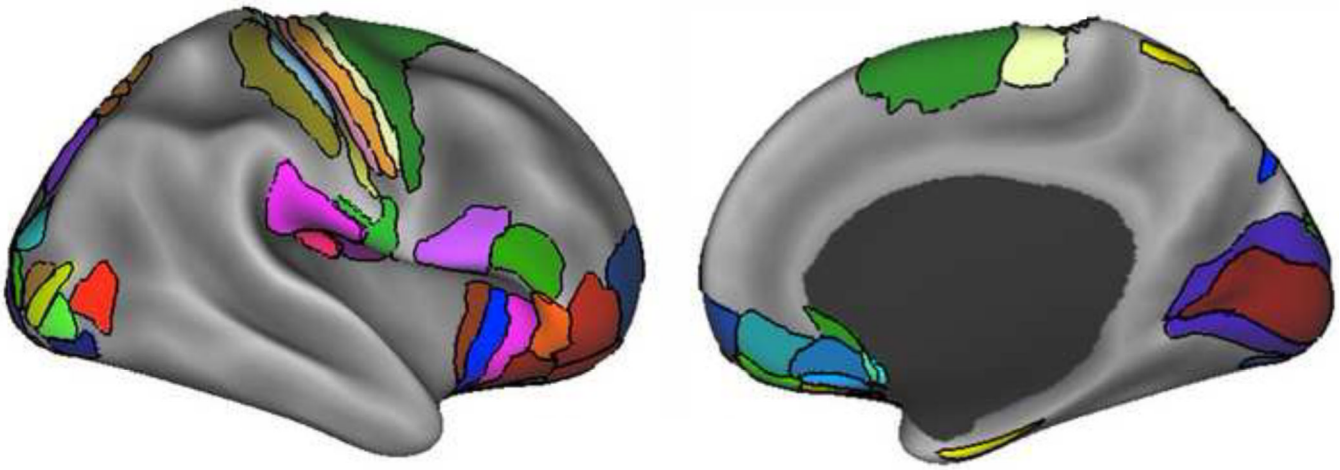

Figure 2.
A map of 52 cortical areas based surface-based analyses of human cerebral cortex and displayed on the fs_LR atlas. Gray areas lack accurate surface-registered maps of well-defined cortical areas. Adapted, with permission, from Van Essen et al. (2011b).

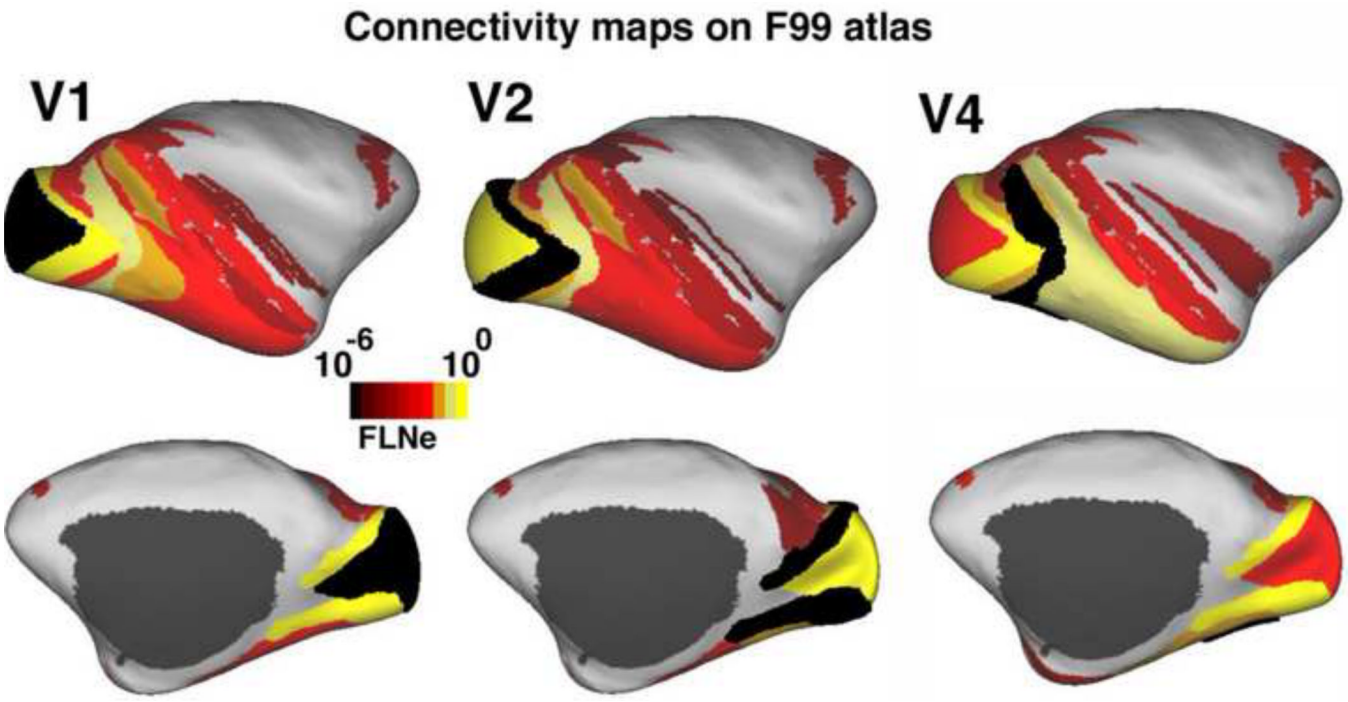

Figure 3.
Projection patterns to areas V1, V2, and V4 revealed by retrograde tracer injections in the macaque. Strength of projections are expressed as FLNe (Fraction of Labeled Neurons extrinsic to the injected area) and shown using a logarithmic scale. Adapted, with permission from Markov et al., 2011.

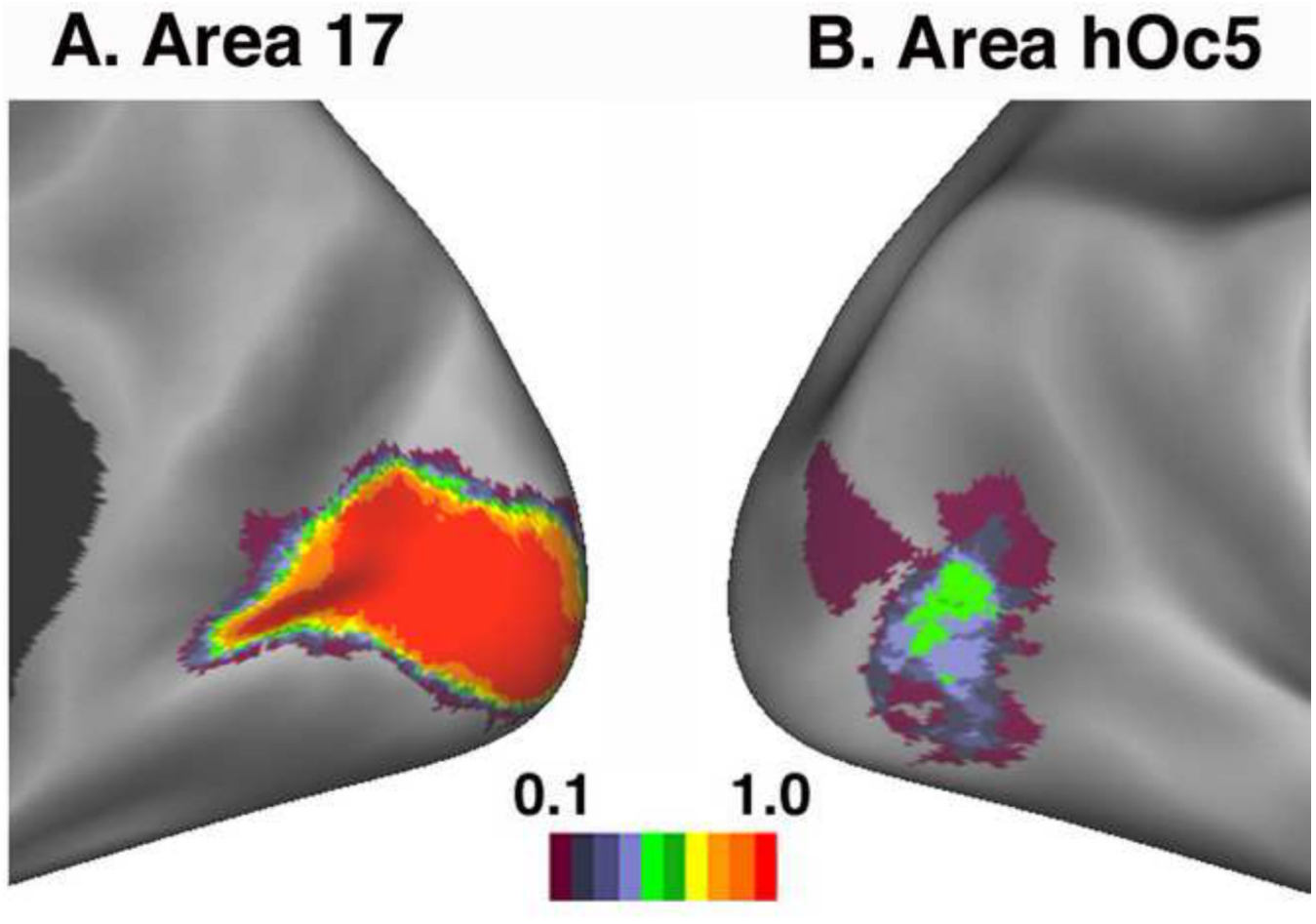

Figure 4.

Regional differences in intersubject alignment of probabilistic architectonic maps achieved by FreeSurfer's surface-based registration algorithm (Fischl et al., 2008; Van Essen et al., 2011b). A. Alignment of area 17 in the calcarine sulcus achieves perfect overlap (red = overlap fraction of 1) over most of area 17's extent. B. Overlap for architectonic area hOc5 (putative area MT) in nearby lateral occipito-temporal cortex is nowhere better than 50% (green = overlap fraction of 0.5), and in many regions there is no overlap of the 10 subjects (indigo = overlap fraction of 0.1).

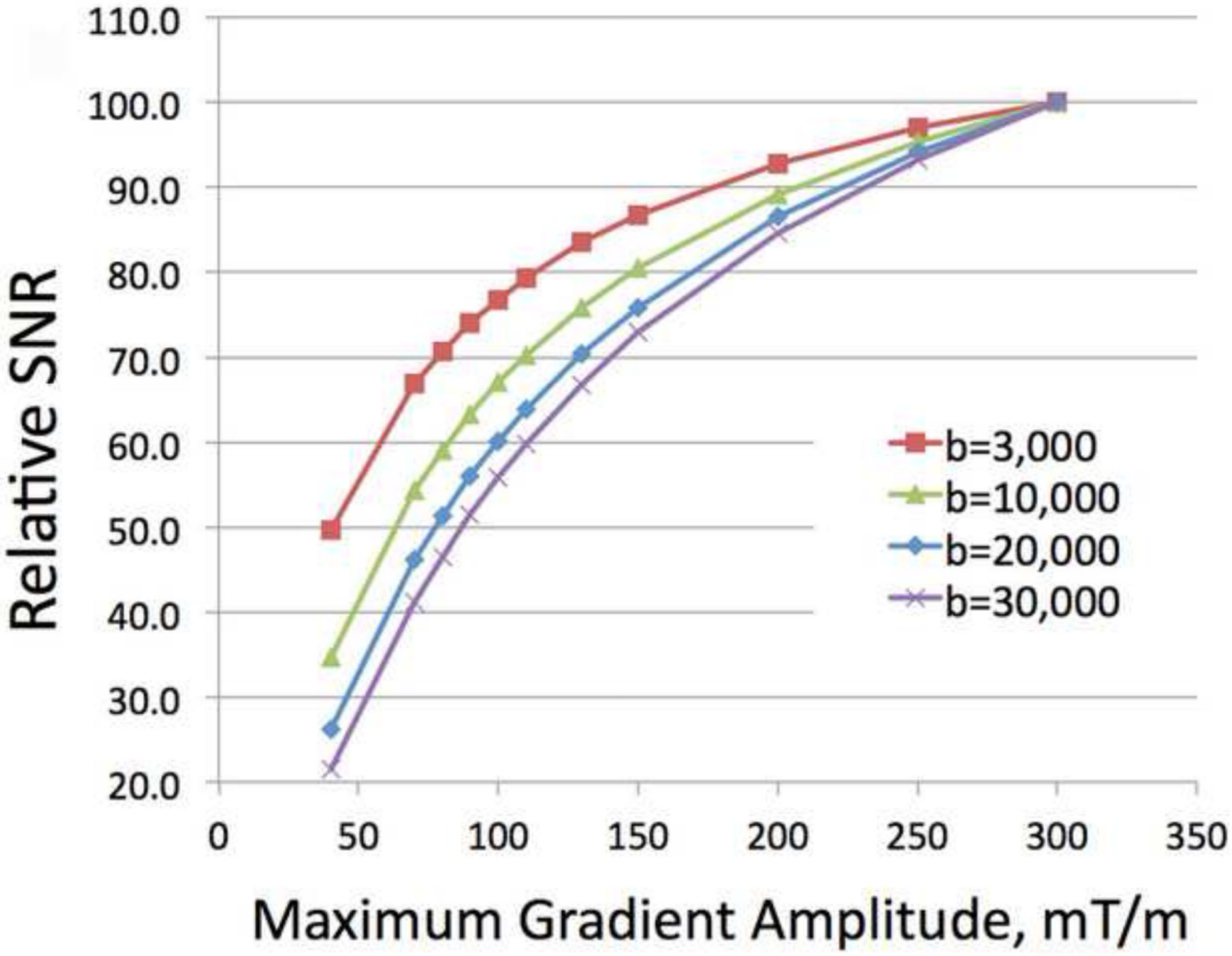

Figure 5.

Relative SNR as a function of maximum gradient strength that can be attained by shortening the diffusion encoding time. Theoretical data points are based on a monopolar diffusion encoding scheme for four different b values (assuming instantaneous rise times). The value of b=20,000 s/mm^2 is likely at the extreme of values to be utilized; current diffusion scans for tractography typically employ b values less than 3000 s/mm^2. A minimum TE of 15 ms due to RF pulses and partial k-space coverage before the peak of the echo is assumed.

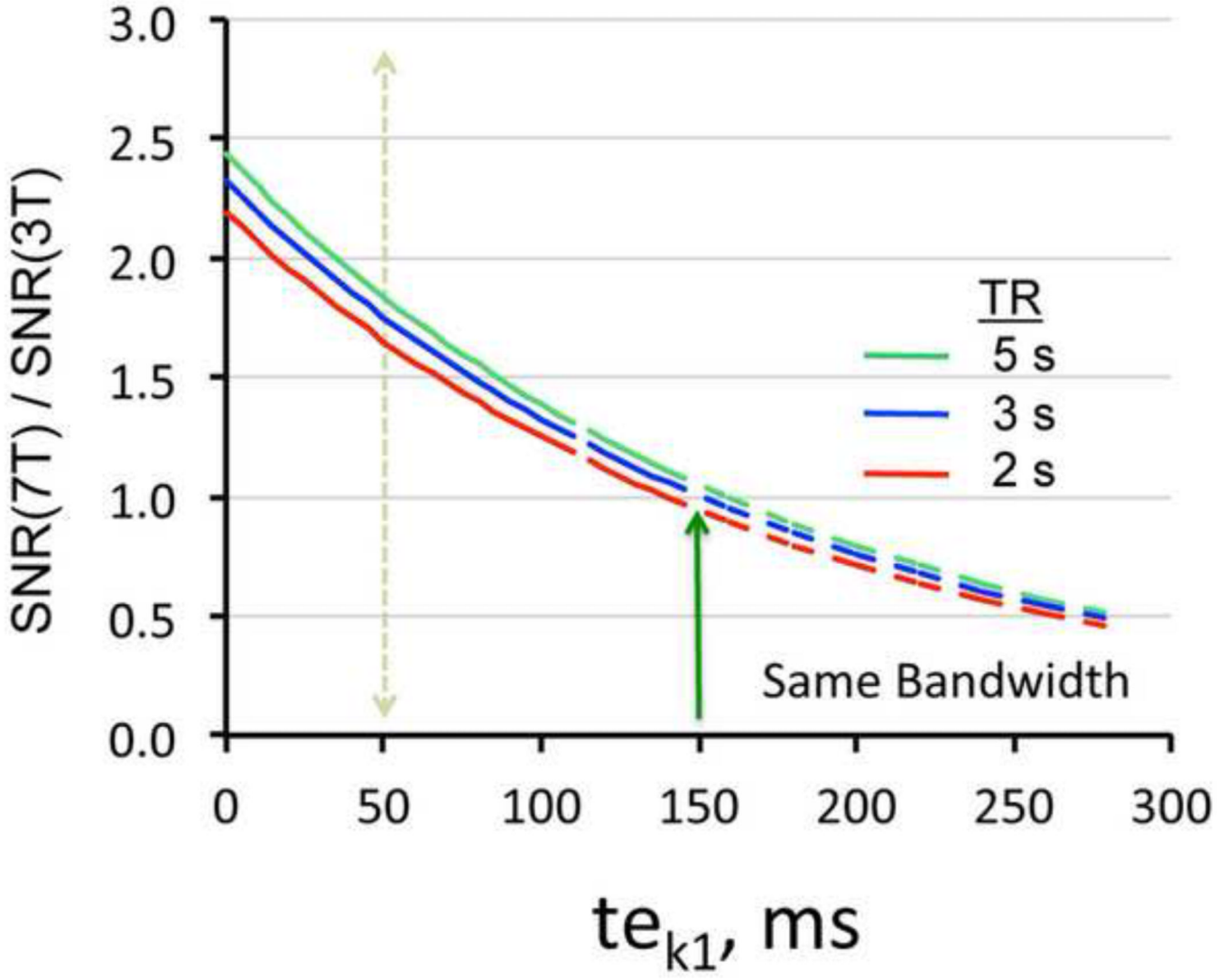

Figure 6.

Ratio of 7T SNR relative to 3T SNR for the central k-space point, k_o, calculated for a spin echo sequence (90 deg. excitation and a single 180 deg. refocusing pulse) as a function of te_{k1}, the time to the first k-space point. 6/8 Partial Fourier EPI acquisition was modeled. The echo time TE is equal to te_{k1} plus the time to acquire 2/8 k-space points to reach the ko signal where maximum echo amplitude occurs. Note that for the above graph, TE>0 even when te_{k1}=0 which accounts for the less than approximately linear gain in SNR at te_{k1}=0 . T1 of white matter was taken as 0.838 s at 3T (Wansapura et al., 1999) and 1.22 s at 7T (Rooney et al., 2007). Bandwidth was kept the same. The minimum TE was taken as 15 ms. The T2 at 3T was reported to be between 55 and 69 ms (Stanisz et al., 2005 and references therein); for these calculations, it was assumed to be the average of this range, i.e. 62 ms. The 7T white matter T2 was taken as 45 ms (Yacoub et al., 2003). Intrinsic SNR was scaled 1.15 times the magnetic field as previously shown experimentally and by modeling (Vaughan et al., 2001). Same matrix size at 3T and 7T was assumed.

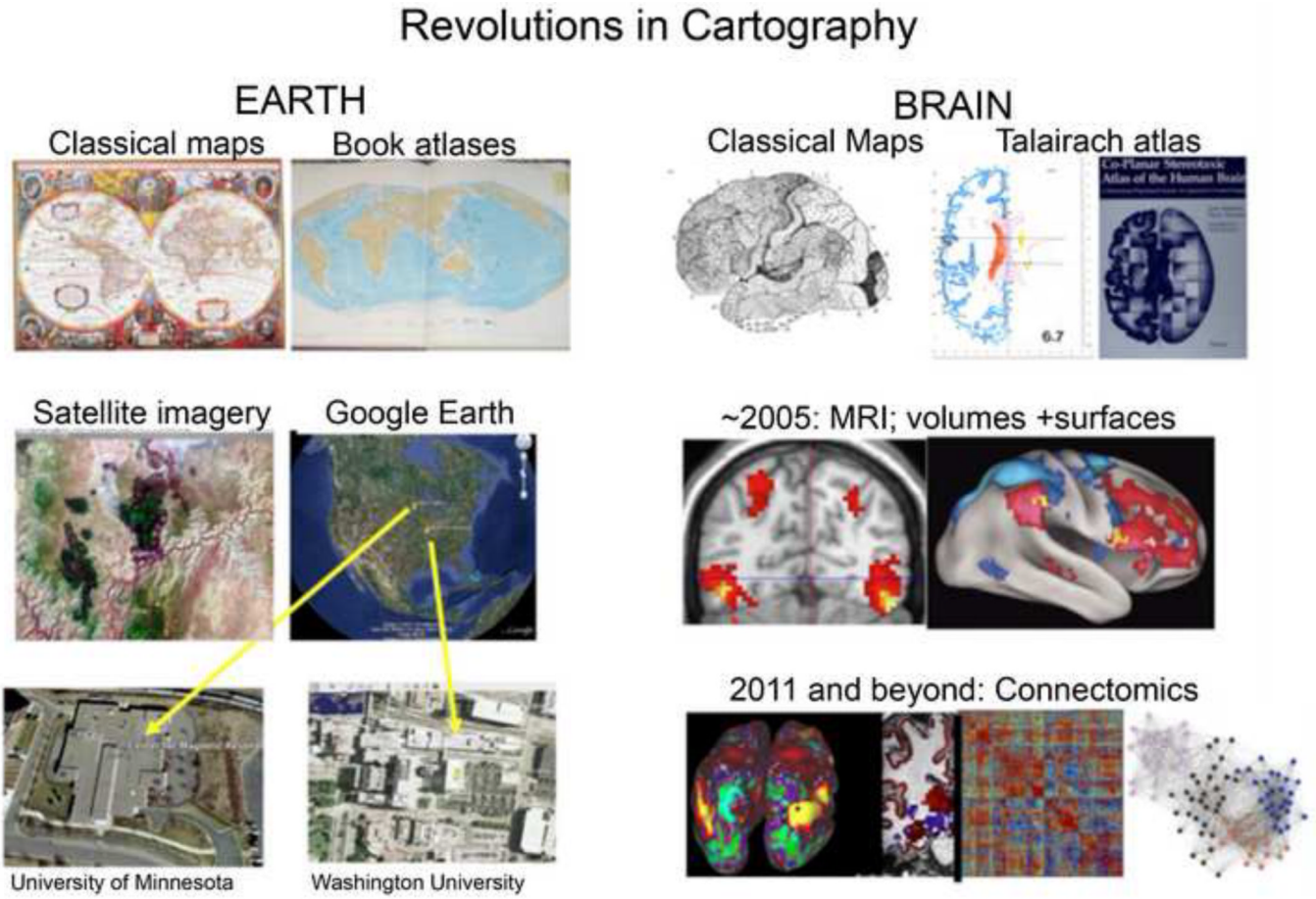

Figure 7.
Revolutions in cartography of the earth's surface (left) and the human brain (right).

Table 1

Human brain numbers

	Cerebral cortex (both hemispheres)	Cerebellum	Subcortical	White Matter	Ventricles/CSF
Surface area Thickness	1,956 cm^2 *[1]* 2.44 mm *[1]*	~1,100 cm^2 *[2]* ~1 mm			
Volume *[3]*	543 cm^3	103 cm^3	78 cm^3 *[4]*	410 cm^3	17 cm^3
# Parcels	~300 – 400 *[1]*	20 - 50? *[5]*	~150 *[6]*		
# Neurons; axon length	1.8×10^{10} cells *[7]*	7×10^{10} cells *[7]*	7×10^{8} cells *[7]*	1.6×10^{10} cm *[8]*	
Density of neurons Density of axons Density of synapses	$9 \times 10^{4}/mm^2$ *[9]* $\sim 3 \times 10^{8}/mm^3$ *[12]*	$7 \times 10^{5}/mm^2$ *[9]*	$1.4 \times 10^{4}/mm^3$ *[10]*	$\sim 3 \times 10^{5}/mm^2$ *[11]*	

References, notes

[1] Van Essen et al. (2011b, Table 1), based on surface areas of 69 individuals in native dimensions.

[2] Sultan and Braitenberg (1993); thickness estimate (volume/surface) is consistent with histology (https://www.msu.edu/~brains/brains/)

[3] Volumes were computed from FreeSurfer segmentation of 69 brains registered to MNI space (Glasser and Van Essen, 2011; total volume 1596 cm^3) but were reduced by a factor of 0.72 (total volume 1149 cm^3) to adjust for the larger size (24% in surface area, 38% in volume) of the MNI atlas relative to individual brains (Table 2, Van Essen et al., 2011b).

[4] 59 cm^3 for telencephalon and diencephalon; 19 cm^3 for brainstem.

[5] Buckner et al., 2011

[6] J.L. Price, personal communication; Mai et al., 2007

[7] Azevedo et al. (2009)

[8] Pakkenberg et al (2003)

[9] Average neuronal density expressed per square mm for cerebral and cerebellar cortex, based on #neurons/surface area. For neocortex, there are large regional variations in neuronal density (Collins et al., 2010).

[10] Neuronal density per mm^3 for subcortical

[11] Average axonal density (per unit cross-sectional area) = total axonal length divided by white-matter-volume

[12] 1.5×10^{14} synapses [8] divided by 5×10^{5} mm^3